# SDSS-V Robotic Focal Plane System: Overview of Coordinate Systems and Transforms.

Conor Sayres<sup>a</sup>, José R. Sánchez-Gallego<sup>a</sup>, Michael R. Blanton<sup>b</sup>, Michael Engelman<sup>c</sup>, Douglas P. Finkbeiner<sup>d</sup>, David W. Hogg<sup>b</sup>, Jon A. Holtzman<sup>e</sup>, Colby Jurgenson<sup>d</sup>, Richard W. Pogge<sup>c</sup>, Solange Ramírez<sup>g</sup>, Andrew K. Saydjari<sup>d</sup>, Edward F. Schlafly<sup>f</sup>, and Sarah Tuttle<sup>a</sup>

<sup>a</sup>Department of Astronomy, University of Washington, Box 351580, Seattle, WA 98195, USA <sup>b</sup>Center for Cosmology and Particle Physics, Department of Physics, New York University, 726 Broadway, New York, NY 10003, USA

<br/>  $^{\rm c}$  Department of Astronomy, Ohio State University, 140 West 18th Avenue, Columbus, O<br/>H43210-1173

<sup>d</sup>Harvard-Smithsonian Center for Astrophysics, 60 Garden St., Cambridge, MA 02138, USA
 <sup>e</sup>Department of Astronomy, New Mexico State University, Las Cruces, NM, 88003, USA
 <sup>f</sup>Lawrence Livermore National Labratory, 7000 East Ave., Livermore, CA, 94550, USA
 <sup>g</sup>Carnegie Observatories, 813 Santa Barbara Street, Pasadena, CA, 91101

## ABSTRACT

The Sloan Digital Sky Survey V (SDSS-V) is an all-sky spectroscopic survey of >6 million objects, designed to decode the history of the Milky Way, reveal the inner working of the stars, investigate the origin of solar systems, and track the growth of supermassive black holes across the Universe. Here we describe the mathematical framework behind the SDSS-V robotic Focal Plane System (FPS), specifically the coordinate systems and transforms used to propagate locations of targets from astronomical catalogs to coordinates on a robotically positioned fiber or guide camera. This framework provides the backbone for the design and operations of SDSS-V's MOS surveys. All coordinate systems and transformations between them are provided in SDSS-V's coordio software package.

## 1. INTRODUCTION

For decades the Sloan Digital Sky Survey (SDSS<sup>1</sup>) has collected multi-object spectroscopy (MOS) using a plug plate system. This system required the manual plugging of plug plates by day and the manual swapping of plug plates between science exposures by night. Since SDSS operations began circa 2000, ~5.6 million unique astronomical sources have been spectroscopically observed using plug plates.

SDSS-V<sup>2</sup> is the fifth iteration of SDSS MOS surveys, and new instrumentation has brought huge shifts in the way SDSS operates.<sup>3</sup> Two Focal Plane Systems (FPS<sup>4</sup>) have been built to replace SDSS plug plates with robotically-positioned fibers. These new instruments reconfigure fibers on short time scales and drastically reduce observational overheads when compared to plug plate operations. SDSS-V's FPS instruments will more than double the number of targets observed in SDSS history over the course of a five year survey.

The first FPS was recently commissioned at Apache Point Observatory's 2.5m Sloan Telescope,<sup>5</sup> and the second instrument has just been shipped to Las Campanas Observatory's 2.5m du Pont Telescope.<sup>6</sup> Each FPS consists of 500 robotic fiber positioners, 6 guide-focus-acquisition (GFA) cameras, and 60 fixed fiducials mounted upon a dished surface termed the "wok". The wok's top surface has been machined to match the telescope's very slight focal plane curvature such that GFAs and science fibers remain in focus across the telescope's field of view. The top panel in Figure 1 shows the unpopulated wok prior to assembly, and the bottom panel shows a solid model rendering of the fully populated wok. The overlaid yellow axes indicate the fundamental coordinate system for the FPS instrument (wok coordinates).

The primary focus of this work is to (1) calculate where a spectroscopic target lands in wok coordinates, and (2) determine the robot's  $(\theta_{\alpha}, \theta_{\beta})$  positioner coordinates that will align a science fiber with that source. The calculation for determining a guide star's location on a GFA chip will proceed along analogous lines. Figure 2

shows the stack of coordinate systems and conversions we have defined for this task, and the mathematics for the complete traversal this stack are detailed in Sections 2 - 8.

Accurate metrology is a prerequisite for accurate coordinate transforms. We need precise knowledge of the location and orientation of a robot or GFA on the wok, and we need precise knowledge of where a fiber is on a robot. Much effort has been devoted to making these measurements using combinations of microscopy, full-wok imaging, lab calibration, and on-sky calibration. Our understanding of the instrument continues to evolve, and we currently estimate that the various elements in the wok are known to  $\sim 10~\mu m$ . Fiber positioning has continued to improve at APO largely due to improvements in our ability to measure where a fiber is.

At the telescope back illuminated fiducial and metrology fibers are measured with a Fiber Viewing Camera (FVC). FVC measurements are used to iteratively correct a robot's  $(\theta_{\alpha}, \theta_{\beta})$  orientation after a blind move. The FVC transform is still being tweaked at APO, and is yet undefined for LCO. The derivation of the FVC transform is complicated enough to deserve a dedicated paper, and it is not discussed further beyond the mention it receives here. Ref. 7 provides an overview of the SDSS-V FVC design.

The complete suite of FPS transforms (in both forward and reverse directions) have been implemented in SDSS-V's coordio\* software package. coordio is written in Python and Python-wrapped C/C++. It provides a common backbone for many other SDSS-V software products including those concerned with survey design and target assignment<sup>†</sup>, robot path planning,<sup>8</sup> and nightly operations<sup>‡</sup>. coordio makes use of SOFA<sup>§</sup> routines for certain astronomical calculations.



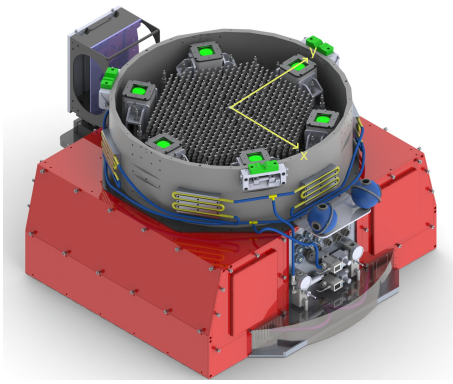


Figure 1: Top panel: the bare wok mounting plate. Bottom panel: solid model rendering of instrument after robots, fiducials, and GFAs have been mounted in the wok. Wok coordinate axes are indicated in yellow.

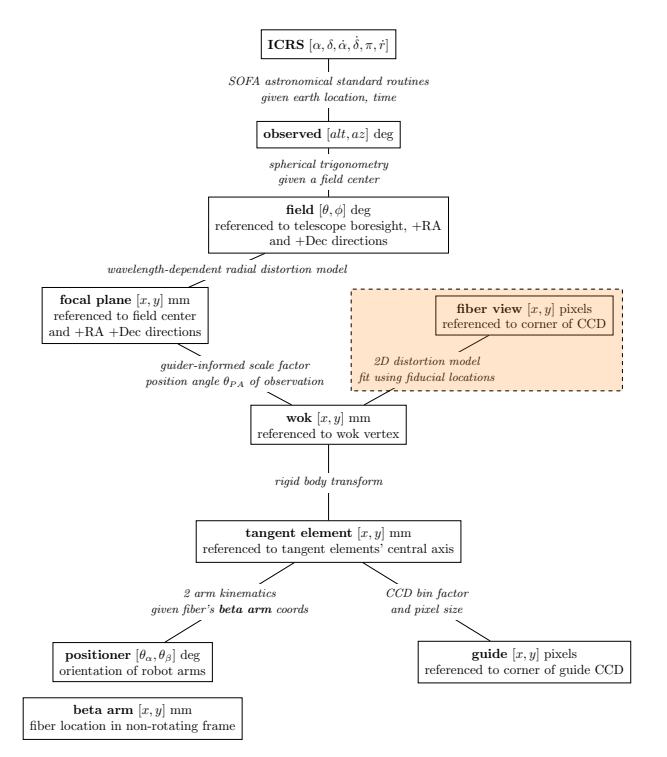


Figure 2: The coordinate transformation stack for the SDSS-V FPS. Coordinate systems are boxed nodes, and edges represent a transform between coordinate systems. The transform between fiber view and wok coordinates (dashed) continues to evolve and not discussed in this manuscript.

<sup>\*</sup>https://github.com/sdss/coordio

<sup>†</sup>https://github.com/sdss/robostrategy

<sup>&</sup>lt;sup>‡</sup>https://github.com/sdss/jaeger

<sup>§</sup>https://www.iausofa.org/

## 2. CATALOG (ICRS) TO OBSERVED (ALT, AZ) COORDINATES

SDSS-V targets are selected from published astronomical catalogs. Prior to observation each target must be associated with (1) a site (APO or LCO), (2) a field center (telescope pointing, or boresight), and (3) a specific fiber on a robot. Both target and boresight ICRS coordinates are converted to observed (Alt, Az) coordinates using SOFA's iauAtco13 routine which handles refraction, proper motion, parallax, Earth orientation, nutation, etc. The relevant inputs and outputs of this calculation are shown in Table 1. Figure 3 shows an example of target and boresight coordinates in the observed coordinate system.

	Inputs					
ra	ICRS right ascension at J2000.0					
$\operatorname{dec}$	ICRS declination at J2000.0					
pmra	RA proper motion					
$\operatorname{pmdec}$	Dec proper motion					
px	parallax					
$\operatorname{rv}$	radial velocity					
lat	latitude of site					
lon	longitude of site					
el	elevation of site					
epoch	time of observation					
wl	wavelength of observation					
$^{\mathrm{rh}}$	relative humidity					
$_{\mathrm{temp}}$	temperature					
	Outputs					
Alt	Altitude angle positive above the horizon					

Azimuthal angle measured eastward from north

Telescope Boresight

On Target

On Morth

North

West

Figure 3: The observed (Alt, Az) coordinate system. NCP is north celestial pole.

Table 1: iauAtco13 inputs and outputs

# 3. OBSERVED (ALT, AZ) TO FIELD $(\phi_{FC}, \theta_{FC})$ COORDINATES

Field coordinates are a spherical coordinate system that specify the location of a target with respect to the telescope boresight.  $\phi_{FC}$  is the angular on-sky separation between the boresight and the target.  $\theta_{FC}$  is the on-sky direction from the boresight to the target, measured from +RA through +Dec. The conversion from observed to field coordinates involves constructing a 3D rotation matrix  $M_B$  derived from the boresight's observed coordinates:

$$\theta_B = -Az_B + 2\pi \tag{1}$$

$$\phi_B = \frac{\pi}{2} - \text{Alt}_B \tag{2}$$

$$M_{1} = \begin{bmatrix} \cos(\frac{\pi}{2} + \theta_{B}) & \sin(\frac{\pi}{2} + \theta_{B}) & 0\\ -\sin(\frac{\pi}{2} + \theta_{B}) & \cos(\frac{\pi}{2} + \theta_{B}) & 0\\ 0 & 0 & 1 \end{bmatrix}$$
(3)

$$M_{2} = \begin{bmatrix} 1 & 0 & 0 \\ 0 & \cos(\phi_{B}) & \sin(\phi_{B}) \\ 0 & -\sin(\phi_{B}) & \cos(\phi_{B}) \end{bmatrix}$$
(4)

$$M_3 = \begin{bmatrix} \cos(q) & \sin(q) & 0\\ -\sin(q) & \cos(q) & 0\\ 0 & 0 & 1 \end{bmatrix}$$
 (5)

$$M_B = M_3 M_2 M_1 \tag{6}$$

(7)

The parallactic angle q in Equation 5 is computed using SOFA's iauHd2pa routine. Figure 4 plots the series of coordinate system rotations  $M_1$ ,  $M_2$ , and  $M_3$ . Figure 5 shows the end result of the coordinate system rotation when viewed along the boresight direction: +y' points along +Dec and +x' points along +RA.

Finally, to convert a target from observed to field coordinates:

$$\theta_T = -Az_T + 2\pi \tag{8}$$

$$\phi_T = \frac{\pi}{2} - \text{Alt}_{\text{T}} \tag{9}$$

$$\begin{bmatrix} x_T \\ y_T \\ z_T \end{bmatrix} = \begin{bmatrix} \cos(\theta_T)\sin(\phi_T) \\ \sin(\theta_T)\sin(\phi_T) \\ \cos(\phi_T) \end{bmatrix}$$
(10)

$$\begin{bmatrix} x_T' \\ y_T' \\ z_T' \end{bmatrix} = M_B \begin{bmatrix} x_T \\ y_T \\ z_T \end{bmatrix}$$
(11)

$$\begin{bmatrix} \phi_{FC} \\ \theta_{FC} \end{bmatrix} = \begin{bmatrix} \arccos(z_T') \\ \arctan 2(y_T', x_T') \end{bmatrix}$$
 (12)

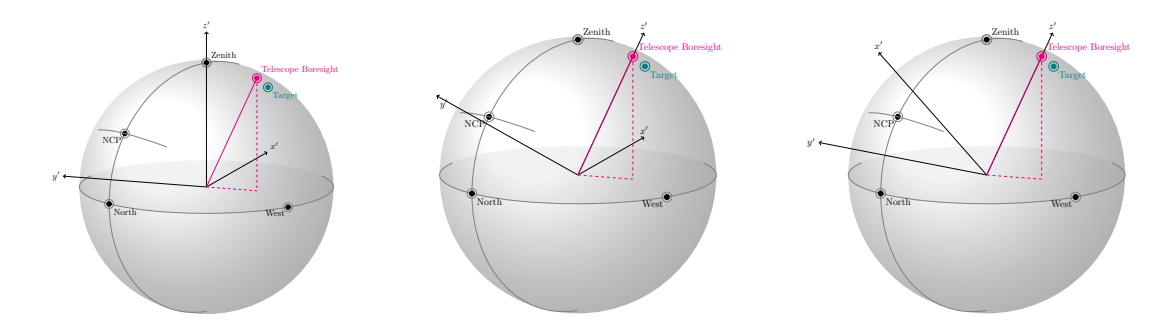


Figure 4: Left:  $M_1$  rotation. Center:  $M_2M_1$  rotation. Right:  $M_3M_2M_1$  rotation.

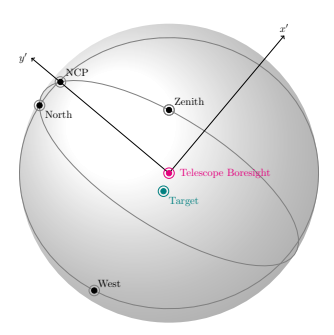


Figure 5:  $M_3M_2M_1$  rotation viewed along the boresight direction.

# 4. FIELD $(\phi_{FC}, \theta_{FC})$ TO FOCAL PLANE $(X_{FPC}, Y_{FPC})$ COORDINATES

Focal plane coordinates are 2D Cartesian with units of mm. +x points along +RA and +y points along +Dec. Figure 6 shows the geometric relationship between field and focal plane coordinates. Converting from field to focal plane coordinates involves a wavelength-dependent radial distortion model. The focal plane is modeled as a spherical surface projected onto the xy plane. The incoming field angle  $\phi_{FC}$  is related to the outgoing focal

plane angle  $\phi'_{FPC}$  by an odd-order polynomial. The conversion from field coordinates to focal plane coordinates is given by:

$$\phi_{FPC}' = c_0 \phi_{FC} + c_1 \phi_{FC}^3 + c_2 \phi_{FC}^5 + c_3 \phi_{FC}^7 + c_4 \phi_{FC}^9$$
(13)

$$\phi'_{FPC} = c_0 \phi_{FC} + c_1 \phi_{FC}^3 + c_2 \phi_{FC}^5 + c_3 \phi_{FC}^7 + c_4 \phi_{FC}^9$$

$$\begin{bmatrix} x_{FPC} \\ y_{FPC} \end{bmatrix} = R \sin(\pi - \phi'_{FPC}) \begin{bmatrix} \cos(\theta_{FC}) \\ \sin(\theta_{FC}) \end{bmatrix}$$
(13)

Polynomial coefficients and focal plane surface radii were determined by least squares fits to ZEMAX ray traces for each telescope at several wavelengths of interest. These parameters are tabulated in Table 2. Polynomial coefficients were calculated for  $\phi_{FC}$  and  $\phi'_{FPC}$  in degrees. The model is only valid for  $\phi_{FC} < 1.5^{\circ}$  at APO and  $\phi_{FC} < 1.1^{\circ}$  at LCO.

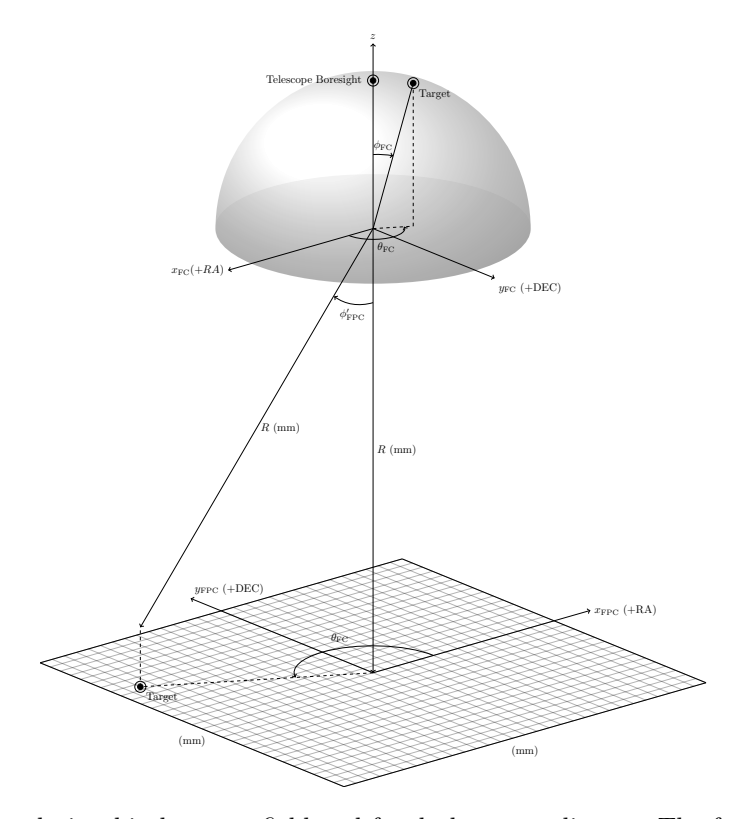


Figure 6: The geometric relationship between field and focal plane coordinates. The focal plane angle  $\phi'_{FPC}$  is a polynomial function of field angle  $\phi_{FC}$ . The focal plane is modeled as a spherical surface with radius R and projected onto the xy plane.

Table 2: Focal Plane Distortion Model Parameters

site	$\lambda (\mu m)$	R  (mm)	$c_0$	$c_1$	$c_2$	$c_3$	$c_4$
APO	1.66	8939	1.40708	6.13779e-03	7.25138e-04	-3.28007e-06	-1.65995e-05
APO	0.54	9208	1.36580	6.09425 e-03	6.54926 e- 04	2.62176e-05	-2.27106e-05
APO	0.6231	9164	1.37239	6.09825 e-03	6.67511e-04	2.14437e-05	-2.17330e-05
LCO	1.66	8905	2.11890	1.40826e-02	1.27996e-04	6.99967e-05	0
LCO	0.54	9938	1.89824	1.31773e-02	1.04445e-04	5.77341e-05	0
LCO	0.6231	9743	1.93618	1.33536e-02	9.17031e-05	6.58945 e - 05	0

# 5. FOCAL PLANE $(X_{FPC}, Y_{FPC})$ TO WOK $(X_{WOK}, Y_{WOK})$ COORDINATES

Wok coordinates are 2D Cartesian with units of mm. Generally, +x points between GFA3 and GFA4 and +y points toward GFA2 (right panel Figure 1). Technically, the wok coordinate axes are defined by the grid of xy fiducial locations for which precise CMM measurements were obtained.

The conversion from focal plane to wok coordinates involves a rotation by  $\theta_{PA}$  (the desired position angle of observation) and a scale. Scale is measured and applied throughout the night using GFA camera feedback. Figure 7 shows the relationship between focal plane and wok coordinates. The conversion defined as:

$$\begin{bmatrix} x_{\text{wok}} \\ y_{\text{wok}} \end{bmatrix} = \frac{1}{\text{scale}} \begin{bmatrix} \cos(\theta_{PA}) & \sin(\theta_{PA}) \\ -\sin(\theta_{PA}) & \cos(\theta_{PA}) \end{bmatrix} \begin{bmatrix} x_{FPC} \\ y_{FPC} \end{bmatrix}$$
(15)

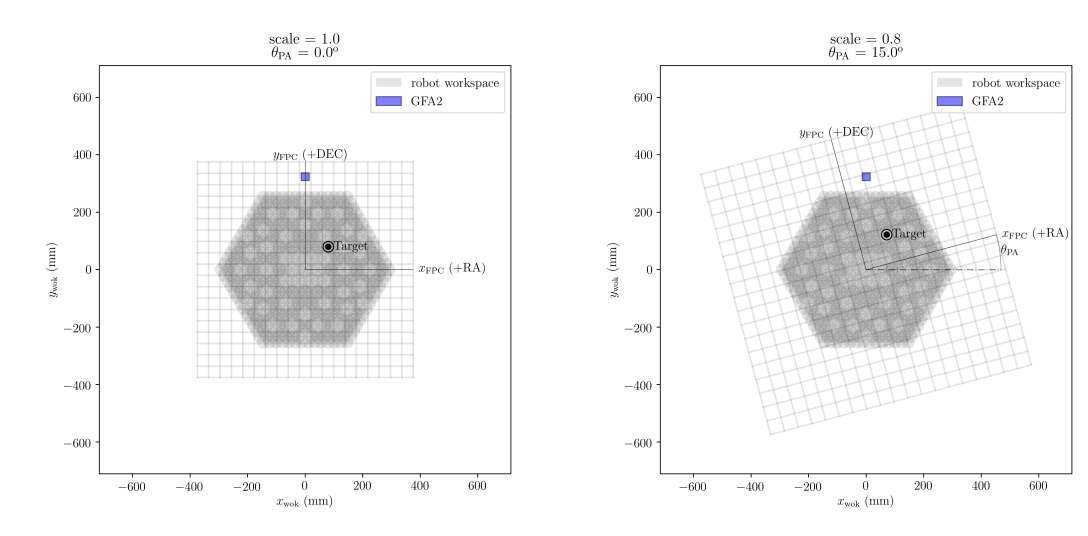


Figure 7: Wok coordinates are related to focal plane coordinates by a rotation (desired position angle) and scale. Small variations in scale are tracked and adjusted throughout the night using the GFA camera on-sky measurements.

## 6. WOK $(X_{WOK}, Y_{WOK})$ TO TANGENT $(X_{TC}, Y_{TC})$ COORDINATES

Tangent coordinates are 2D Cartesian with units of mm. Each element on the wok has a unique tangent coordinate system. The tangent coordinate origin is located at either (1) the center of a robot's work space or (2) the center of a GFA CCD. The transform from wok to tangent coordinates is given by:

$$\begin{bmatrix} \mathbf{x}_{TC} \\ \mathbf{y}_{TC} \end{bmatrix} = \begin{bmatrix} -\hat{x} - \\ -\hat{y} - \end{bmatrix} \begin{pmatrix} \begin{bmatrix} \mathbf{x}_{wok} \\ \mathbf{y}_{wok} \end{bmatrix} - \begin{bmatrix} x_b \\ y_b \end{bmatrix}$$
 (16)

where  $\hat{x}$  and  $\hat{y}$  are orthogonal unit vectors that specify the direction of the tangent x and y axes in wok coordinates, and  $(x_b, y_b)$  specify the origin of the tangent element in wok coordinates. For positioners  $\hat{x}$  points along the  $\theta_{\alpha} = 0$  axis, which is  $\sim [0, -1]$  for all positioners. For GFAs  $\hat{x}$  is parallel to CCD rows.  $\hat{x}$  is is  $\sim [1, 0]$  for GFA2 and  $\sim [-1, 0]$  for GFA5. The precise values for  $\hat{x}$ ,  $\hat{y}$ ,  $x_b$ , and  $y_b$  are carefully measured for each robot and GFA installed in the wok.

# 7. TANGENT $(X_{TC}, Y_{TC})$ TO GUIDE $(X_{CCD}, Y_{CCD})$ COORDINATES

Guide coordinates are 2D Cartesian with units of pixels. The origin of the guide coordinate frame is the lower left corner of the lower left pixel of the CCD. The GFA CCDs are (2048,2048) square devices with 13.5  $\mu$ m pixels. The tangent to guide coordinate conversion is specified as:

$$x_{CCD} = \frac{1}{\sin_x} \left[ \frac{1000}{13.5} x_{TC} + 2048/2 \right]$$
 (17)

$$y_{CCD} = \frac{1}{\sin_y} \left[ \frac{1000}{13.5} y_{TC} + 2048/2 \right]$$
 (18)

where  $bin_x$  and  $bin_y$  are the column and row CCD bin factors.

## 8. POSITIONER $(\theta_{\alpha}, \theta_{\beta})$ TO TANGENT $(X_{TC}, Y_{TC})$ COORDINATES

Positioner coordinates are specified by two angles  $(\theta_{\alpha}, \theta_{\beta})$ .  $\theta_{\alpha}$  is a rotation about the robot's alpha axis,  $\theta_{\beta}$  is a rotation about the robot's beta axis. The alpha and beta axes are separated by a length  $l_{\alpha} \sim 7.4$  mm (a measured quantity for each robot). Figure 8 shows the orientation of robot arms and the axes of rotation. The wok coordinate frame and tangent coordinate frame are indicated in the figure. The robot's alpha and beta arms are unequal lengths, which leads to an annular patrol zone for fibers carried in the beta arm.

Each robot carries three fibers on beta arm: a metrology fiber, an APOGEE fiber, and a BOSS fiber. Fiber coordinates are specified in the beta arm frame  $(x_{\beta}, y_{\beta})$  in mm. By definition, the origin of the beta arm frame is at the beta axis of rotation and +x points to the metrology fiber center. Fiber positions in the beta arm frame are shown in Figure 9.

The forward kinematic equation defining the location of a fiber in tangent coordinates is:

$$\theta_F = \arctan 2(y_\beta, x_\beta) \tag{19}$$

$$r_F = \sqrt{x_\beta^2 + y_\beta^2} \tag{20}$$

$$\begin{bmatrix} x_{TC} \\ y_{TC} \end{bmatrix} = \begin{bmatrix} \cos(\theta_{\alpha}) & \cos(\theta_{\alpha} + \theta_{\beta} + \theta_{F}) \\ \sin(\theta_{\alpha}) & \sin(\theta_{\alpha} + \theta_{\beta} + \theta_{F}) \end{bmatrix} \begin{bmatrix} l_{\alpha} \\ r_{F} \end{bmatrix}$$
(21)

(22)

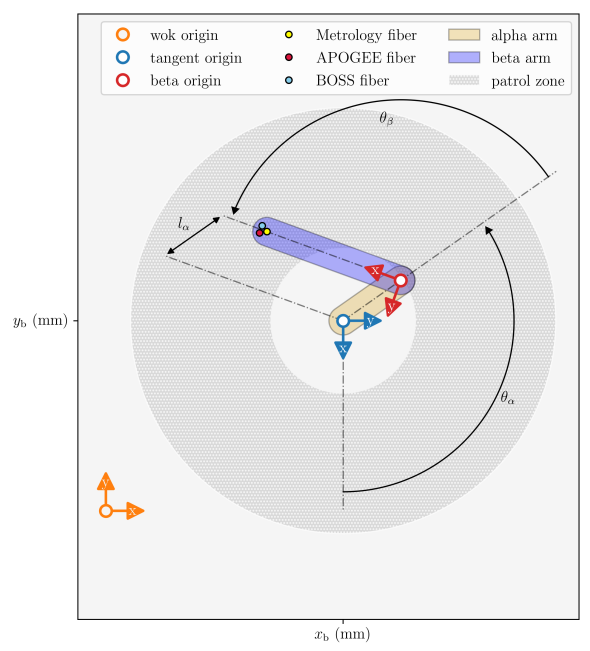


Figure 8: Two arm kinematics for SDSS-V robots.  $\theta_{\alpha}$  is the rotation of the alpha arm,  $\theta_{\beta}$  is the rotation of the beta arm. Wok and tangent coordinate frames are indicated by orange and blue axes. Red axes indicate the beta arm coordinate frame.

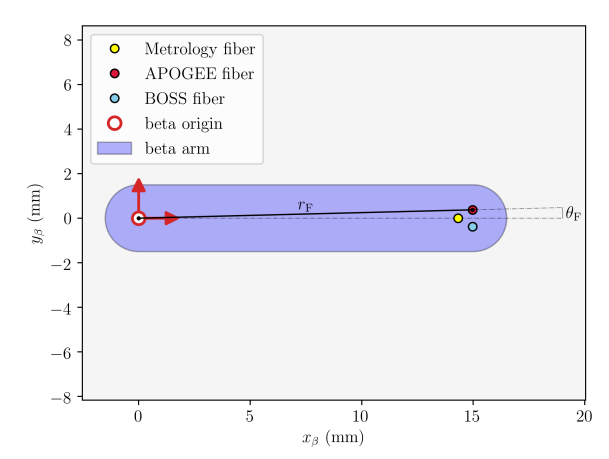


Figure 9: The beta arm coordinate frame. Origin is set to the center of beta arm rotation, +x points to the metrology fiber.  $(x_{\beta}, y_{\beta})$  fiber locations in mm are specified in this frame.

#### 9. DISCUSSION AND CONCLUSION

Omitting the FVC, this work shows the complete suite of coordinate systems and transforms SDSS-V has chosen for survey design and operations with the FPS instruments. The coordinate system mapping is shown graphically in Figure 2 and mathematically in Sections 2 - 8. In each section, the transform is only shown in one direction. Most of the transforms we have derived are algebraically invertible, with the exception of a few that deserve mention.

In Section 2, the reverse transform from (Alt, Az) observed coordinates to ICRS coordinates directly employs SOFA's iauAtoc13 routine. In Section 4, the reverse transform from  $(x_{FPC}, x_{FPC})$  focal plane coordinates to  $(\phi_{FC}, \theta_{FC})$  field coordinates involves a separate set of polynomial coefficients  $c_0$ - $c_4$  to compute:

$$\phi_{FC} = c_0 \phi'_{FPC} + c_1 \phi'^3_{FPC} + c_2 \phi'^5_{FPC} + c_3 \phi'^7_{FPC} + c_4 \phi'^9_{FPC}$$
(23)

In Section 8, it is of common interest to compute the inverse kinematics:  $(\theta_{\alpha}, \theta_{\beta})$  positioner coordinates given  $(x_{TC}, y_{TC})$  tangent coordinates. Solutions to this problem only exist for  $(x_{TC}, y_{TC})$  points within the robot's workspace. To solve this we have employed the Algorithm 2RIK which is described online.

A self-contained technical description of coordinate systems and their transformations has both organized and simplified SDSS survey planning and operations code. SDSS-V's coordio software package has implemented coordinate transforms as described here, allowing conversions between any two coordinate systems in the stack. coordio has become a key tool used throughout the SDSS-V survey's growing code base. This document should aid anyone with interest in SDSS-V codes, or perhaps inspire software designs for similar instruments.

 $<sup>\</sup>P$ https://motion.cs.illinois.edu/RoboticSystems/InverseKinematics.html

#### ACKNOWLEDGMENTS

The authors thank Kris Hauser for his online notes related to robotic systems https://motion.cs.illinois.edu/RoboticSystems/.

Funding for the Sloan Digital Sky Survey V has been provided by the Alfred P. Sloan Foundation, the Heising-Simons Foundation, and the Participating Institutions. SDSS acknowledges support and resources from the Center for High-Performance Computing at the University of Utah. The SDSS web site is www.sdss5.org.

SDSS is managed by the Astrophysical Research Consortium for the Participating Institutions of the SDSS Collaboration, including the Carnegie Institution for Science, Chilean National Time Allocation Committee (CNTAC) ratified researchers, the Gotham Participation Group, Harvard University, Heidelberg University, The Johns Hopkins University, L'Ecole polytechnique fédérale de Lausanne (EPFL), Leibniz-Institut für Astrophysik Potsdam (AIP), Max-Planck-Institut für Astronomie (MPIA Heidelberg), Max-Planck-Institut für Extraterrestrische Physik (MPE), Nanjing University, National Astronomical Observatories of China (NAOC), New Mexico State University, The Ohio State University, Pennsylvania State University, Smithsonian Astrophysical Observatory, Space Telescope Science Institute (STScI), the Stellar Astrophysics Participation Group, Universidad Nacional Autónoma de México, University of Arizona, University of Colorado Boulder, University of Illinois at Urbana-Champaign, University of Toronto, University of Utah, University of Virginia, Yale University, and Yunnan University.

## REFERENCES

- [1] York, D. G., Adelman, J., John E. Anderson, J., Anderson, S. F., Annis, J., Bahcall, N. A., Bakken, J. A., Barkhouser, R., Bastian, S., Berman, E., Boroski, W. N., Bracker, S., Briegel, C., Briggs, J. W., Brinkmann, J., Brunner, R., Burles, S., Carey, L., Carr, M. A., Castander, F. J., Chen, B., Colestock, P. L., Connolly, A. J., Crocker, J. H., Csabai, I., Czarapata, P. C., Davis, J. E., Doi, M., Dombeck, T., Eisenstein, D., Ellman, N., Elms, B. R., Evans, M. L., Fan, X., Federwitz, G. R., Fiscelli, L., Friedman, S., Frieman, J. A., Fukugita, M., Gillespie, B., Gunn, J. E., Gurbani, V. K., de Haas, E., Haldeman, M., Harris, F. H., Hayes, J., Heckman, T. M., Hennessy, G. S., Hindsley, R. B., Holm, S., Holmgren, D. J., hao Huang, C., Hull, C., Husby, D., Ichikawa, S.-I., Ichikawa, T., Ivezić, Ž., Kent, S., Kim, R. S. J., Kinney, E., Klaene, M., Kleinman, A. N., Kleinman, S., Knapp, G. R., Korienek, J., Kron, R. G., Kunszt, P. Z., Lamb, D. Q., Lee, B., Leger, R. F., Limmongkol, S., Lindenmeyer, C., Long, D. C., Loomis, C., Loveday, J., Lucinio, R., Lupton, R. H., MacKinnon, B., Mannery, E. J., Mantsch, P. M., Margon, B., McGehee, P., McKay, T. A., Meiksin, A., Merelli, A., Monet, D. G., Munn, J. A., Narayanan, V. K., Nash, T., Neilsen, E., Neswold, R., Newberg, H. J., Nichol, R. C., Nicinski, T., Nonino, M., Okada, N., Okamura, S., Ostriker, J. P., Owen, R., Pauls, A. G., Peoples, J., Peterson, R. L., Petravick, D., Pier, J. R., Pope, A., Pordes, R., Prosapio, A., Rechenmacher, R., Quinn, T. R., Richards, G. T., Richmond, M. W., Rivetta, C. H., Rockosi, C. M., Ruthmansdorfer, K., Sandford, D., Schlegel, D. J., Schneider, D. P., Sekiguchi, M., Sergey, G., Shimasaku, K., Siegmund, W. A., Smee, S., Smith, J. A., Snedden, S., Stone, R., Stoughton, C., Strauss, M. A., Stubbs, C., SubbaRao, M., Szalay, A. S., Szapudi, I., Szokoly, G. P., Thakar, A. R., Tremonti, C., Tucker, D. L., Uomoto, A., Berk, D. V., Vogeley, M. S., Waddell, P., i Wang, S., Watanabe, M., Weinberg, D. H., Yanny, B., and Yasuda, N., "The sloan digital sky survey: Technical summary," The Astronomical Journal 120, 1579–1587 (sep 2000).
- [2] Kollmeier, J. A., Zasowski, G., Rix, H.-W., Johns, M., Anderson, S. F., Drory, N., Johnson, J. A., Pogge, R. W., Bird, J. C., Blanc, G. A., Brownstein, J. R., Crane, J. D., De Lee, N. M., Klaene, M. A., Kreckel, K., MacDonald, N., Merloni, A., Ness, M. K., O'Brien, T., Sanchez-Gallego, J. R., Sayres, C. C., Shen, Y., Thakar, A. R., Tkachenko, A., Aerts, C., Blanton, M. R., Eisenstein, D. J., Holtzman, J. A., Maoz, D., Nandra, K., Rockosi, C., Weinberg, D. H., Bovy, J., Casey, A. R., Chaname, J., Clerc, N., Conroy, C., Eracleous, M., Gänsicke, B. T., Hekker, S., Horne, K., Kauffmann, J., McQuinn, K. B. W., Pellegrini, E. W., Schinnerer, E., Schlafly, E. F., Schwope, A. D., Seibert, M., Teske, J. K., and van Saders, J. L., "SDSS-V: Pioneering Panoptic Spectroscopy," arXiv e-prints, arXiv:1711.03234 (Nov 2017).
- [3] Sánchez-Gallego, J. R., Sayres, C., Donor, J., Toro, A. A., Araujo, R., Kronig, L., Grossen, L., Pogge, R., Wachter, S., Ramírez, S., and Brownstein, J., "Multi-object spectroscopic operations with the Sloan Digital Sky Survey V," in [Observatory Operations: Strategies, Processes, and Systems VIII], Adler, D. S., Seaman, R. L., and Benn, C. R., eds., 11449, 83 96, International Society for Optics and Photonics, SPIE (2020).

- [4] Pogge, R. W., Derwent, M. A., O'Brien, T. P., Jurgenson, C. A., Pappalardo, D., Engelman, M., Brandon, C., Brady, J., Clawson, N., Shover, J., Mason, J., Kneib, J.-P., Araujo, R., Bouri, M., Kronig, L., Grossen, L., Gillet, D., Macktoobian, M., Tuttle, S. E., Farr, E., Sánchez-Gallego, J., and Sayres, C., "A robotic Focal Plane System (FPS) for the Sloan Digital Sky Survey V," in [Society of Photo-Optical Instrumentation Engineers (SPIE) Conference Series], Society of Photo-Optical Instrumentation Engineers (SPIE) Conference Series 11447, 1144781 (Dec. 2020).
- [5] Gunn, J. E., Siegmund, W. A., Mannery, E. J., Owen, R. E., Hull, C. L., Leger, R. F., Carey, L. N., Knapp, G. R., York, D. G., Boroski, W. N., Kent, S. M., Lupton, R. H., Rockosi, C. M., Evans, M. L., Waddell, P., Anderson, J. E., Annis, J., Barentine, J. C., Bartoszek, L. M., Bastian, S., Bracker, S. B., Brewington, H. J., Briegel, C. I., Brinkmann, J., Brown, Y. J., Carr, M. A., Czarapata, P. C., Drennan, C. C., Dombeck, T., Federwitz, G. R., Gillespie, B. A., Gonzales, C., Hansen, S. U., Harvanek, M., Hayes, J., Jordan, W., Kinney, E., Klaene, M., Kleinman, S. J., Kron, R. G., Kresinski, J., Lee, G., Limmongkol, S., Lindenmeyer, C. W., Long, D. C., Loomis, C. L., McGehee, P. M., Mantsch, P. M., Neilsen, Jr., E. H., Neswold, R. M., Newman, P. R., Nitta, A., Peoples, Jr., J., Pier, J. R., Prieto, P. S., Prosapio, A., Rivetta, C., Schneider, D. P., Snedden, S., and Wang, S.-i., "The 2.5 m Telescope of the Sloan Digital Sky Survey," AJ 131, 2332–2359 (Apr. 2006).
- [6] Bowen, I. S. and Vaughan, Jr., A. H., "The optical design of the 40-in. telescope and of the Irénée DuPont telescope at Las Campanas Observatory, Chile.," AO) 12, 1430–1434 (1973).
- [7] Jurgenson, C., Engelman, M., Pogge, R., O'Brien, T., Pappalardo, D., Clawson, N., Derwent, M., Brandon, C., Mason, J., Brady, J., and Shover, J., "SDSS-V focal plane robot positioning metrology," in [Society of Photo-Optical Instrumentation Engineers (SPIE) Conference Series], Society of Photo-Optical Instrumentation Engineers (SPIE) Conference Series 11447, 1144780 (Dec. 2020).
- [8] Sayres, C., Sánchez-Gallego, J. R., Blanton, M. R., Araujo, R., Bouri, M., Grossen, L., Kneib, J.-P., Kollmeier, J. A., Kronig, L., Pogge, R. W., and Tuttle, S., "SDSS-V Algorithms: Fast, Collision-free Trajectory Planning for Heavily Overlapping Robotic Fiber Positioners," AJ 161, 92 (Feb. 2021).